NANO LETTERS

Letter

pubs.acs.org/NanoLett

Engineered Si Electrode Nanoarchitecture: A Scalable Postfabrication Treatment for the Production of Next-Generation Li-Ion Batteries

Fathy M Hassan,[†] Victor Chabot,[†] Abdel Rahman Elsayed,[†] Xingcheng Xiao,*[,‡] and Zhongwei Chen*[,†]

[†]Department of Chemical Engineering, University of Waterloo, Waterloo, Ontario N2L3G1, Canada

[‡]Chemical Sciences and Materials Systems, General Motors Global Research and Development Center, Warren, Michigan 48090, United States

Supporting Information

ABSTRACT: A novel, economical flash heat treatment of the fabricated silicon based electrodes is introduced to boost the performance and cycle capability of Li-ion batteries. The treatment reveals a high mass fraction of Si, improved interfacial contact, synergistic SiO_2/C coating, and a conductive cellular network for improved conductivity, as well as flexibility for stress compensation. The enhanced electrodes achieve a first cycle efficiency of ~84% and a maximum charge capacity of 3525 mA h g^{-1}, almost 84% of silicon's theoretical maximum. Further, a stable reversible charge capacity of 1150 mA h g^{-1} at 1.2 A g^{-1} can be achieved over 500 cycles. Thus, the flash heat treatment method introduces a promising avenue for the production of industrially viable, next-generation Li-ion batteries.

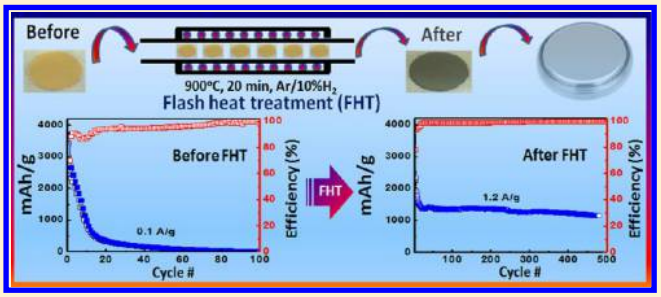

KEYWORDS: *Nanostructures, silicon, lithium-ion battery, flash heat treatment, rate capability, electrochemical performance*

The pursuit of high performance lithium-ion battery (LIB) materials is critical for applications including electric vehicles, consumer electronics, and the storage of renewable energy. This requires a new generation of electrode materials with higher energy density and long cycle life, without compromising low production costs, safety, or the scalability necessary for commercial deployment.[1−5] Silicon (Si) has emerged as a strong candidate to replace graphite as the anode material in commercial LIB design.[6] Its appeal arises from a high theoretical storage capacity of ~4200 mA h g^{-1}, natural abundance and low cost, and low working potential 0−0.4 V vs Li/Li^+.[7,8] However, the extreme volume change (~400%) experienced during lithiation/delithiation results in pulverization of the silicon and loss of the electrical connection, leading to rapid capacity loss.[9−12] In addition, the solid electrolyte interphase (SEI) layer on the Si surface, which has to bear the same volume expansion and contraction, will also crack, fracture, or delaminate from the Si, leading to low Columbic efficiency.[6]

To inhibit expansion and overcome this limitation, one of the most attractive strategies is to tailor the nanostructure and buffer the mechanical strain by preparing Si/C composites, dispersing silicon particles within or coating them with a porous carbon.[12−17] These techniques intend to improve cycle stability of Si, minimize direct exposure of Si to electrolyte to improve current efficiency, and enhance the electrical connection between Si and C. In a different strategy, Si-based electrodes can be directly prepared by the inclusion of commercial Si nanoparticles mixed into a functional polymer binding matrix.[18−23] In addition, the covalent linkages between the binder and the SiO_2 surface layer on the Si particles can mitigate the mechanical damage caused by severe volume change, while providing an elastic network that extends throughout the entire electrode and maintains the electrodes' integrity. However, these techniques are sensitive to: the dispersion quality of the active materials, a physically bonded Si−C interface that becomes ineffective after cycling, and the high inactive carbon/binder content required to achieve stable capacity.[24−27]

Progressively, higher performance and more durable configurations have been achieved by utilizing sophisticated methodologies to produce Si and Si@carbon core−shell nanowires,[28−33] as well as porous composite structures coated with Si nanoparticles.[34−36] However, most of these reports utilize SiH_4, an expensive and extremely hazardous gas, and delicate multistep treatments of synthesized nanostructured silicon. Controlled growth of SiO_2 coatings on these materials have also been shown to significantly decrease volume expansion, improving capacity retention during cycling when the coating was optimized to between 2 and 10 nm.[37,38] For comparison, a recent report by Wang et al. reveals nanowire performance retaining 1100 mA h g^{-1} after 1000 cycles.[39] This is in agreement with previous investigation onto the carbon coating of Si particles, prior to cell assembly, which suggests the

Received: October 21, 2013
Revised: November 25, 2013
Published: December 12, 2013

   dx.doi.org/10.1021/nl403943g | *Nano Lett.* 2014, 14, 277−283

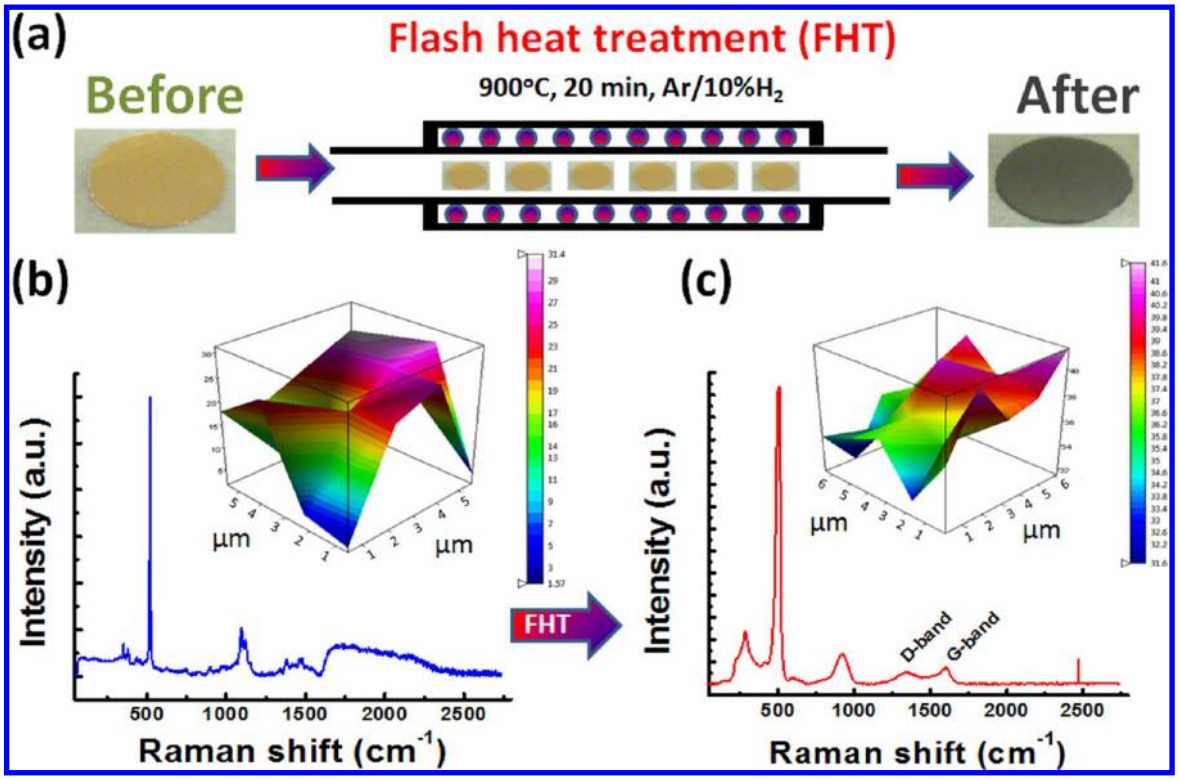

Figure 1. (a) Schematic of the flash heat treatment process (FHT) showing optical micrographs for the electrode surface before and after FHT and the Raman spectrum for the electrode surface both, (b) before FHT and (c) after FHT. The insets in b and c correspond to Raman mapping of the fwhm of the Si peak.

main advantage of PVDF is the localized reaction between HF leached during carbonization and SiO_2, thereby controlling layer thickness.[40−42]

In this present work, we present a safe, economical, and short duration strategy for post-treatment of Si electrodes made with commercially available Si nanaoparticles (Si-NP) to achieve high-performance. The single-step flash heat treatment (FHT) process, which simultaneously engineered the electrode matrix and the surface architecture of Si, is compatible with continuous roll-to-roll electrode processing. To our knowledge, this is the first time that the direct engineering of the electrode structure by the rapid post-treatment of commercial Si particles has been reported to be successful. Specifically, the benefits of the FHT postprocess include: (1) the creation of a SiO_2/C shell around the Si-NP which restricts volume expansion and stabilizes the SEI layer; (2) the carbonized binder generates a dense cellular network throughout the entire electrode, interconnecting the Si particles, boosting the electrical conductivity, and attributing to the enhanced electrode integrity; and (3) manipulation of the copper current collector to catalyze graphene growth, resulting in a strong interfacial contact mechanically and electrically. In addition, all of the binders were converted into graphitic carbon, which should give the electrode much better durability in the electrochemical environment. Also, the dispersion of Si powder in the binder before the FHT treatment would be much better since no conductive additive is needed. All of those synergetic functions contribute to the significantly improved performance in terms of cycle stability and rate capability (500 cycles, retaining capacity of 1150 mA h g^{-1} at a high discharge rate of 1.2 A g^{-1}).

Figure 1 illustrates FHT of the as-prepared Si-NP/PVDF (60/40 wt %) electrode on copper foil, in addition to the impact on electrode structure. The FHT process is detailed within the Experimental Section and briefly involves moving the electrodes through a high temperature furnace purged with a mixture of $Ar_{(g)}$ and $H_{2(g)}$, at a constant rate. The high ramp results in carbonization of the polymer matrix starting at ∼450 °C (thermal gravimetric analysis (TGA), Figure S1), also determined by the visual change in color of the electrodes from a light brown to black. For practical manufacturing consideration, after FHT the Si content within the electrodes increased to 87.2 wt %, and no deflagration of the electrode occurred. The electrode materials, prepared by FHT, result in an electrode structure with good adherence to the current collector and with excellent flexibility (not brittle). This is clearly demonstrated in Figure S2, whereby we subjected one of the FHT electrodes to bending. No rupture or microcrack formation arising from the tensile stress was observed. This flexibility was attributed to the polymer carbonization leading to an interconnected carbon network with a coherent, intact structure. This is supported by a recent study by Chen et al.,[43] whereby they obtained an elastic carbon foam through carbonization of a polymer for use as flexible electrodes. Raman spectroscopy was used to study the change in chemical structure before and after FHT (Figure 1b,c). As expected, a strong peak centered at 520 cm^{-1} was observed for the nontreated electrode, corresponding to the lattice vibration of crystalline silicon. After FHT, this peak broadens and shifts to slightly lower wave numbers; this is attributed to formation of stresses created by a difference in the thermal expansion coefficient between Si and C.[44−47] This stress is determined to be consistent over a large area by mapping the full-width at half-maximum (fwhm) of the silicon peak before and after FHT (insets, Figure 1b,c). In addition, two peaks arise at 283 and

dx.doi.org/10.1021/nl403943g | Nano Lett. 2014, 14, 277−283

927 cm^{-1} after FHT, which may correspond to the Si−O−Si bending and stretching vibrations of silica on the Si-NP surface, respectively.[48,49] Carbonization of the polymer binder is confirmed by the introduction of carbons characteristic D and G band peaks at 1335 cm^{-1} and 1600 cm^{-1}, with an I_d/I_g ratio of 0.72. The shape and position of these peaks is explained by structural disorder and defects within the mostly amorphous carbon.[50−52] Further, several Raman peaks attributed to polyvinylidene fluoride (PVDF) before treatment are no longer present after FHT, as evidenced by the disappearance of the F peak in the energy dispersive X-ray chart of the treated electrode (EDX, Figure S3).

XRD patterns in Figure 2 show the analysis for the electrode surface after FHT (Figure 2a) along with the reference peaks of silicon, copper, and copper silicide. Also, the XRD pattern for the as-received silicon nanoparticles is provided in the Supporting Figure S4. The presence of copper silicide is not unexpected after heating both Si and Cu at 900 °C.[53] However, shielding of the SiNP by carbon should minimize the formation of copper silicide, as judged by the very small peak at a d-spacing of 2.46 A. We believe this only occurs at the current collector interface and that it also may contribute to the good adherence of the electrode coating. Experimentally we obtained a charge capacity equivalent to almost 84% of silicon's theoretical maximum (see later), indicating minimal consumption of Si in side reactions during the FHT process. Comparing Figures 2a and S4, it is interesting to note the phase orientation of Si created by the FHT process. The 111 peak of Si becomes inhibited, and other Si peaks such as 331 were enhanced. In a similar finding, this peak shift was found to be associated with HF etching of Si.[54]

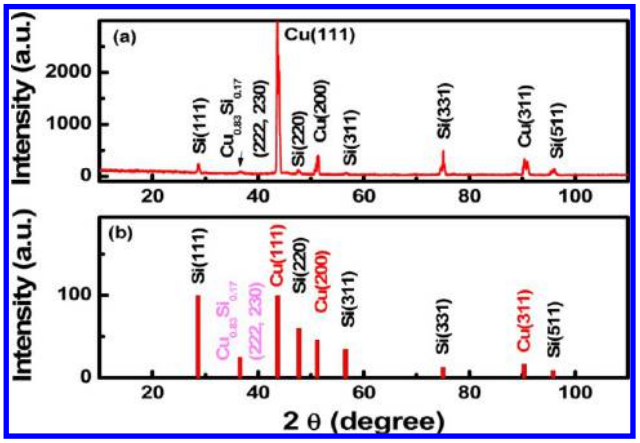

Figure 2. (a) XRD pattern for the electrode surface after FHT and (b) shows the reference peaks of silicon (JCPDS 5-0565), copper (JCPDS 4-0836), and copper silicide (JCPDS 23-0223).

Investigation of the Si-NP surface structure and morphology after FHT is represented by high-resolution TEM and electron energy-loss spectroscopy (EELS) analysis in Figure 3. The dispersed particles remain interconnected by the carbonized PVDF matrix and reveal an amorphous ∼10 nm carbon shell around Si, illustrated by Figure 3a−c. Electron diffraction of a large area (SAED, Figure 3d) confirms that Si remains crystalline after FHT. A native SiO_2 layer is expected on the as-received Si surface;[15,55] however, there is no clear separation between the amorphous SiO_2 and carbon coatings. To accurately map the atomic contributions EELS (Figure 3f), <1 nm spatial resolution,[56] was performed across a particles diameter (Figure 3e, red line). Overlap of the O and C content within the coating suggests that the FHT process forms an entangled coating of SiO_2 and carbon. A similar confirmatory result is found from the energy dispersive spectroscopy (EDS)

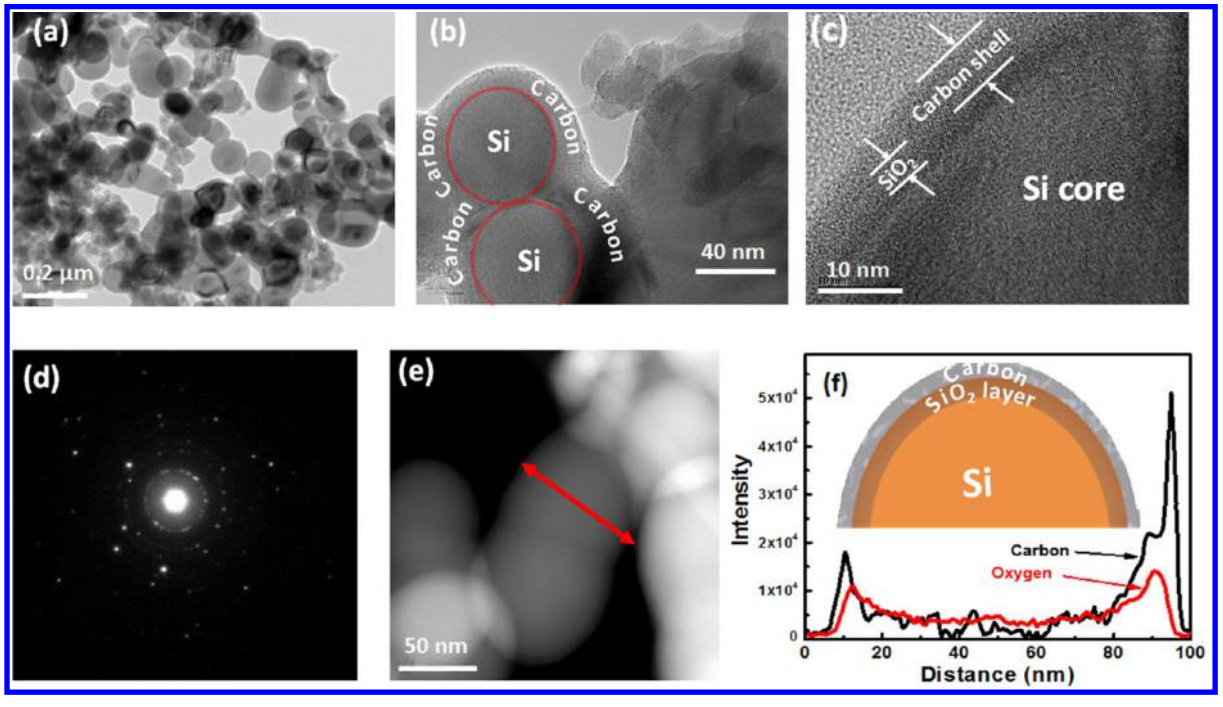

Figure 3. (a) Low-magnification TEM image of the electrode surface after FHT. (b) Higher magnification TEM image zooming to a small area of a, (c) HRTEM image across the edge of one Si particle, (d) selected electron diffraction (SAED) taken from a large area of the electrode surface, (e) a HAADF-STEM image of a few silicon particles on the electrode surface with carbon coating, and (f) electron energy loss spectroscopy (EELS) profile analysis across the particle labeled in e, the inset in f is a schematic depicting the core silicon and the shells of SiO_2 and carbon layer.

dx.doi.org/10.1021/nl403943g | Nano Lett. 2014, 14, 277−283

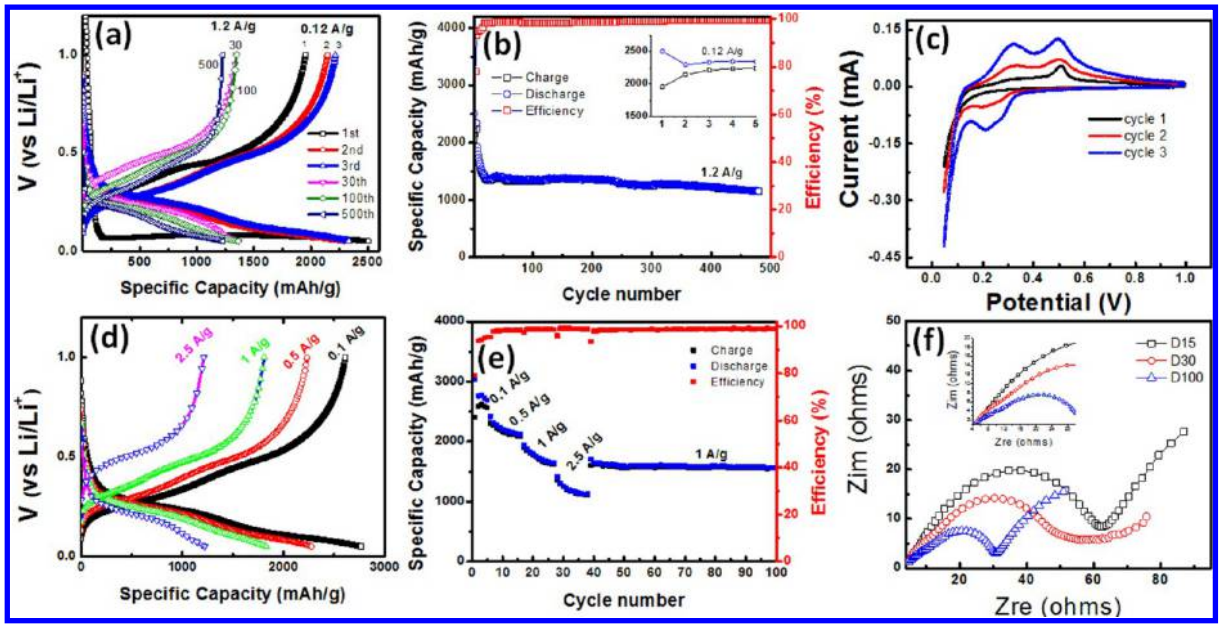

Figure 4. (a) Galvanostatic voltage profile showing cycles 1−3 at 0.12 A g^{-1} and cycles 30, 100, and 500 at 1.2 A g^{-1}, (b) cycle capability for the cell shown in a, (c) cyclic voltamogram for a coin cell measured at scan rate of 0.05 mV s^{-1} between 1.0 and 0.05 V (vs Li^+/Li), (d) galvanostatic voltage profile at different rates, (e) cycle performance showing the rate capability, and (f) EIS for the coin cell after discharge of the cycles 15, 30, and 100.

line scan available in Figure S5. This phenomenon is likely described by the decomposition of the PVDF matrix, releasing traces of HF which are consumed locally due to the partial etching SiO_2.[40−42] It is suspected that this etching regulates the formation of porous SiO_2[57−60] and allows carbon to deposit within the surface cavities created. Practically, the combined SiO_2 and C coating may have a synergistic effect, the higher surface area anchoring the carbon shell and increasing both electrical and ionic conductivity through the SiO_2 layer. In addition, upon cycling the SiO_2 should interact with Li^+, forming a stable $Li_2Si_2O_5$ phase, reported to effectively reduce Si volume expansion.[37,38]

The electrochemical performance of the treated electrode at low current (0.1 A g^{-1}) and a voltage range of 1.5 to 0.005 V is shown in the Supporting Figure S6. It reveals that the FHT treated Si electrode achieves a first cycle efficiency of ∼84% and a maximum charge capacity of 3525 mA h g^{-1} which is almost 84% of the maximum theoretical capacity of silicon. Figure 4 shows the electrochemical performance characterization of the FHT treated electrodes after assembling them into coin cells, using lithium metal as the counter electrode. Cells depicting the voltage profile and durability in Figure 4a,b were initially cycled at 0.12 A g^{-1} from 1 to 0.05 V for 5 cycles, before shifting to a moderately high rate of 1.2 A g^{-1} for long-term testing. First cycle charge and discharge capacities of the coin cells made using the FHT process were 2505 and 1955 mA h g^{-1}, respectively, which corresponds to 78% Coulombic efficiency. The stability of the electrode structure led to reversible discharge capacity of 2240 mA h g^{-1} (1806 mA h cm^{-3}) after 5 cycles at 0.12 A g^{-1} and stable capacity of 1350 mA h g^{-1} after switching to 1.2 A g^{-1}. The effectiveness of the SiO_2/C shell and cellular carbon matrix holding the electrode together is made apparent by the retention of 1150 mA h g^{-1} after 500 cycles, with 99.8% cyclic efficiency. Further, Figure 4d,e illustrate the voltage profile of the FHT treated electrodes in response to varying discharge/charge rates, even at a high rate of 2.5 A g^{-1} the cells began to stabilize after only 10 cycles. This is in sharp contrast to the untreated electrodes (60:20:20 wt %, Si:PVDF:Super-P), which degraded rapidly, retaining only 13.5% of its charge capacity after only 20 cycles at 0.1 A g^{-1} (Figure S7). The improvements for the electrodes subjected to FHT are attributed to improved interfacial contact between the Si and carbon, along with good electronic conductivity throughout the electrode.

To further elucidate lithiation/delithiation stability, cells made with treated electrodes were subjected to both cyclic voltammetry (CV, Figure 4c) and electrochemical impedance spectroscopy (EIS, Figure 4f). Inspection of the first cycle CV for the treated Si electrode reveals that, in the cathodic branch the peak starting at ∼0.15 V corresponds to the conversion of the Si to the Li_xSi phase. The two peaks at ∼0.32 and 0.51 in the anodic branch corresponds to delithiation of the Li_xSi phase to Si. After further cycles, an additional broad peak at ∼0.20 V appears during the cathodic scan, and the anodic peaks at ∼0.32 and 0.51 V become broader and stronger, which is a common characteristic for the transition from crystalline silicon to amorphous silicon due to lithiation/delithiation.[28,61−63] The increasing CV curve area is due to initial activation of the material, enabling more Li to react with Si, which is consistent with both the findings of others[28,64] and our results introduced in Figure 4a,b. The stability of the electrode macrostructure is supported by results of the EIS spectrum taken from cells after discharge cycles 15, 30, and 100, respectively. Extrapolation of the curves semicircular regime reveals that the real charge transfer resistance decreases from 65 Ω after only 15 cycles, to 37 Ω upon completion of 100 cycles. The lower values of ESR reveal that the FHT process renders the electrodes with sufficient conductivity and further confirm the perceived stability of the electrode matrix and the SiO_2/C coating created by the FHT process during electrochemical cycling. The alloying reaction with Si is able to occur more quickly after long-term cell conditioning, and the ESR improvement strongly suggests the stability of the electron and ion pathways which could otherwise impede charge transfer.

After the completion of long-term electrochemical cycling using the FHT processed electrodes, the coin cell was opened

dx.doi.org/10.1021/nl403943g | Nano Lett. 2014, 14, 277−283

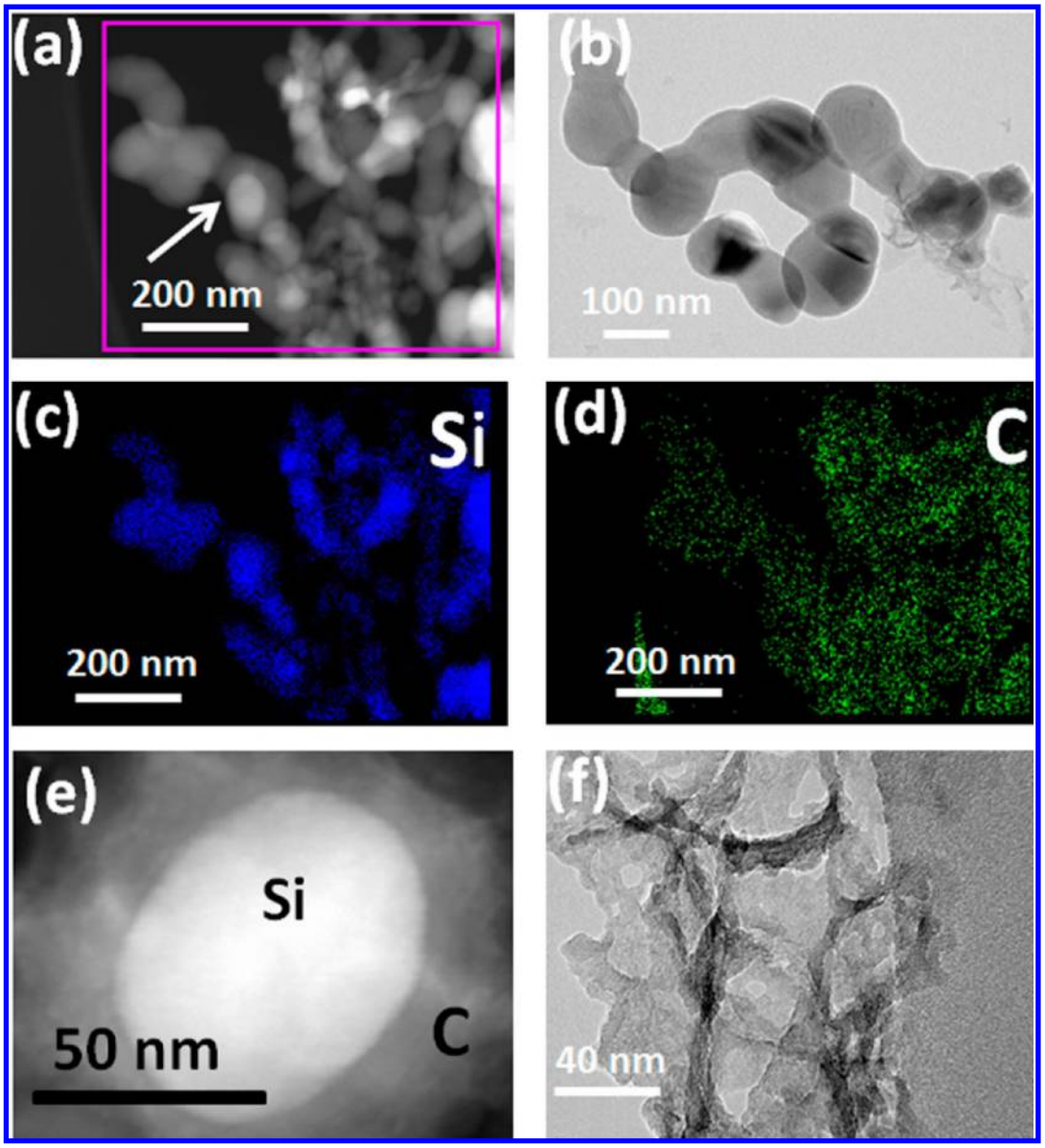

Figure 5. (a) High-angle annular dark field scanning transmission electron micrograph (HAADF-STEM) of the electrode surface after being cycled for 500 cycles of charge/discharge, (b) TEM image showing a few Si particles included in their carbon cage and interconnecting even after 500 cycles, (c and d) EDS elemental mapping of Si and C for the area selected in image a. (e) HAADF-STEM zoomed in to a silicon particle as labeled in a. (f) TEM micrograph for part of the electrode surface after cycling.

to facilitate further investigation of changes to the surface morphology using HAADF-STEM (Figure 5a–e). This figure shows that after 500 cycles the formed amorphous silicon is caged in a sponge-like carbon that persists against expansion and contraction during lithiation/delithiation even after this long cycling. A large area EDS scan reveals the positional mapping of the Si and C distribution (Figure 5c and d, respectively). High resolution of a single representative Si particle suggests the amorphous SiO_2/carbon coating remains in strong contact with the carbon shell. In addition to the stable particle coating, Figure 5f depicts by TEM the detection of graphene-like sheets taken from the electrodes after cycling. The existence of graphene within the treated electrode is supported by literature revealing carbon diffusion into copper can catalyze the formation of monolayer graphene adsorption at high temperatures.[65−70] This suggests that the graphene sheets are assumed to exist on the current collector surface. Further, TEM analysis depicted in Figure S8 confirms graphene sheets are indeed forming during the FHT processing of a copper electrode coated with only PVDF. These results verify that the FHT process is also able to successfully alter the current collector/electrode interface, potentially enhancing electrode stability.

In conclusion, the success of this strategy reveals an elegant approach to solving an old problem, providing a scalable methodology for treating commercial Si particles. The controlled heat treatment provides an effective approach to engineer, in a single step: the interfacial contact with copper, the binding matrix, and the creation of a synergistic SiO_2/C coating. The treated electrodes possess built-in void space for rapid ion transport and successfully retain strong contact between the SiO_2/C shell and the Si-NP, promoting efficient electron transport even after long-term cycling. As a result the enhanced electrodes allow for the controlled expansion of Si

dx.doi.org/10.1021/nl403943g | *Nano Lett.* 2014, 14, 277−283

and achieve high reversible capacity (2240 mA h g^{-1} @ 120 mA g^{-1}), as well as good rate capability and durability (1150 mA h g^{-1} @ 1200 mA g^{-1} over 500 cycles). Further, elimination of binder facilitates high temperature operation in industrial applications which limit the current electrode design standard. The emphasis of a simplified process represents a promising avenue for the production of industrially viable high-performance Si-based electrodes, which could be extended for roll-to-roll manufacturing of next-generation Li-Ion batteries.

Experimental Methods. Electrodes for lithium ion battery testing were fabricated using commercially available silicon nanoparticles (Si-NP) with the size range 50−70 nm purchased from Nanostructured & Amorphous Materials, Inc. (Houston, TX). For the working electrode, a slurry consisting of 60% of active material (Si-NP) and 40% polyvinylidene fluoride (PVdF) as a binder (with no conducting materials added) was prepared in *N*-methyl-2-pyrrolidone (NMP) and was coated on Cu foil. The average mass loading of silicon on the electrodes was 0.5 mg cm^{-2}. The electrode was dried in a convection oven at 353 K for 1 h, followed by drying in the vacuum oven at 363 K for overnight. The electrodes were then subjected to the FHT process; see below. Coin type half cells were fabricated in an argon-filled glovebox with the working electrode and a Li metal counter electrode. A polypropylene separator was employed to separate the two electrodes and the electrolyte composed of 1 M $LiPF_6$ in 30 wt % ethylene carbonate (EC), 60 wt % dimethyl carbonate (DMC), and 10 wt % fluorinated ethylene carbonate (FEC). Galvanostatic charge/discharge test was carried out at a cut off voltage range of 0.05−1.00 V with different current densities for rate capability testing. Cyclic voltammetry, at a scan rate of 0.05 mV s^{-1} between 1.0 and 0.05 V, and electrochemical impedance spectroscopy were conducted using a Princeton Applied Research VersaSTAT MC potentiostat. For a reference coin cell, an electrode was prepared with the ratio of 60 wt % Si-NP, 20% Super-P as a the conductive material, and 20% polyvinylidene fluoride (PVdF) as a binder. These electrodes were used without FHT treatment.

For flash heat treatment (FHT), electrodes were placed into a long quartz tube of a horizontal tube furnace such that they are kept outside the furnace during heating up to 900 °C. Once the temperature reached 900 °C, the quartz tube was cautiously introduced into the furnace for rapid thermal shock of the electrodes, held for 20 min, and then dragged back for rapid cooling. The treatment was performed under gas flow of 100 SCCM Ar/10%H_2.

The morphology of the electrode surfaces before and after treatment was characterized by scanning electron microscopy (SEM) (LEO FESEM 1530) and transmission electron microscopy (TEM) JEOL 2010F TEM/STEM field emission transmission electron microscope, with a large solid angle for high X-ray throughput, scanning, scanning-transmission, and a Gatan imaging filter (GIF) for energy filtered imaging and electron energy loss spectroscopy. Raman scattering spectra were recorded on a Bruker Sentterra system (532 nm laser).

■ ASSOCIATED CONTENT

Supporting Information

Additional figures describing the results of TGA, TEM, SEM, XRD, EDS, cycle stability, and performance analysis. This material is available free of charge via the Internet at http://pubs.acs.org.

■ AUTHOR INFORMATION

Corresponding Authors

*E-mail: xingcheng.xiao@gm.com.

*E-mail: zhwchen@uwaterloo.ca.

Notes

The authors declare no competing financial interest.

■ ACKNOWLEDGMENTS

The authors would like to acknowledge financial support from the Natural Sciences and Engineering Research Council of Canada (NSERC), the University of Waterloo, and the Waterloo Institute for Nanotechnology. TEM, EELS, and HAADF-STEM were obtained at the Canadian Center for Electron Microscopy (CCEM) located at McMaster University. X.C.X. also acknowledges the support by the Assistant Secretary for Energy Efficiency and Renewable Energy, Office of Vehicle Technologies of the U.S. Department of Energy under contract no. DE-AC02-05CH11231, subcontract no. 7056410 under the Batteries for Advanced Transportation Technologies (BATT) Program.

■ ABBREVIATIONS

LIB, lithium-ion battery; FHT, flash heat treatment; SiNP, silicon nanoparticles; fwhm, full-width at half-maximum; pvdf, polyvinylidene fluoride; EELS, electron energy loss spectroscopy; HAADF-STEM, high-angle annular dark field scanning transmission electron micrograph

■ REFERENCES

(1) Hassan, F. M.; Chen, Z.; Yu, A.; Chen, Z.; Xiao, X. *Electrochim. Acta* **2013**, *87*, 844−852.

(2) Liao, J.-Y.; Xiao, X.; Higgins, D.; Lee, D.; Hassan, F.; Chen, Z. *Electrochim. Acta* **2013**, *108*, 104−111.

(3) Liao, J.-Y.; Higgins, D.; Lui, G.; Chabot, V.; Xiao, X.; Chen, Z. *Nano Lett.* **2013**, 5467−5473.

(4) Tarascon, J. M.; Armand, M. *Nature* **2001**, *414*, 359−67.

(5) Armand, M.; Tarascon, J.-M. *Nature* **2008**, *451*, 652−7.

(6) Wu, H.; Cui, Y. *Nano Today* **2012**, *7*, 414−429.

(7) Sharma, R.; Seefurth, R. *J. Electrochem. Soc.* **1976**, *123*, 1763−1768.

(8) Kim, H.; Seo, M.; Park, M.-H.; Cho, J. *Angew. Chem., Int. Ed.* **2010**, *49*, 2146−9.

(9) Beaulieu, L. Y.; Eberman, K. W.; Turner, R. L.; Krause, L. J.; Dahn, J. R. *Electrochem. Solid-State Lett.* **2001**, *4*, A137.

(10) Wu, H.; Cui, Y. *Nano Today* **2012**, *7*, 414−429.

(11) Wu, H.; Chan, G.; Choi, J. W.; Ryu, I.; Yao, Y.; McDowell, M. T.; Lee, S. W.; Jackson, A.; Yang, Y.; Hu, L.; Cui, Y. *Nat. Nanotechnol.* **2012**, *7*, 310−5.

(12) Kasavajjula, U.; Wang, C.; Appleby, A. J. *J. Power Sources* **2007**, *163*, 1003−1039.

(13) Wilson, A.; Dahn, J. *J. Electrochem. Soc.* **1995**, *142*, 326−332.

(14) Gao, P.; Fu, J.; Yang, J.; Lv, R.; Wang, J.; Nuli, Y.; Tang, X. *Phys. Chem. Chem. Phys.* **2009**, *11*, 11101−11105.

(15) Hu, Y.-S.; Demir-Cakan, R.; Titirici, M.-M.; Müller, J.-O.; Schlögl, R.; Antonietti, M.; Maier, J. *Angew. Chem., Int. Ed.* **2008**, *47*, 1645−9.

(16) Demir Cakan, R.; Titirici, M.-M.; Antonietti, M.; Cui, G.; Maier, J.; Hu, Y.-S. *Chem. Commun.* **2008**, 3759−3761.

(17) Ng, S.-H.; Wang, J.; Wexler, D.; Konstantinov, K.; Guo, Z.-P.; Liu, H.-K. *Angew. Chem., Int. Ed.* **2006**, *45*, 6896−6899.

(18) Koo, B.; Kim, H.; Cho, Y.; Lee, K. T.; Choi, N.-S.; Cho, J. *Angew. Chem., Int. Ed.* **2012**, *51*, 8762−7.

(19) Kovalenko, I.; Zdyrko, B.; Magasinski, A.; Hertzberg, B.; Milicev, Z.; Burtovyy, R.; Luzinov, I.; Yushin, G. *Science* **2011**, *334*, 75−79.

(20) Han, Z.-J.; Yabuuchi, N.; Shimomura, K.; Murase, M.; Yui, H.; Komaba, S. *Energy Environ. Sci.* **2012**, *5*, 9014−9020.
(21) Ryou, M.-H.; Kim, J.; Lee, I.; Kim, S.; Jeong, Y. K.; Hong, S.; Ryu, J. H.; Kim, T.-S.; Park, J.-K.; Lee, H.; Choi, J. W. *Adv. Mater.* **2013**, *25*, 1571−6.
(22) Martin, C.; Alias, M.; Christien, F.; Crosnier, O.; Bélanger, D.; Brousse, T. *Adv. Mater.* **2009**, *21*, 4735−4741.
(23) Li, J.; Christensen, L.; Obrovac, M. N.; Hewitt, K. C.; Dahn, J. R. *J. Electrochem. Soc.* **2008**, *155*, A234−A238.
(24) Hochgatterer, N. S.; Schweiger, M. R.; Koller, S.; Raimann, P. R.; Wöhrle, T.; Wurm, C.; Winter, M. *Electrochem. Solid-State Lett.* **2008**, *11*, A76.
(25) Beattie, S. D.; Larcher, D.; Morcrette, M.; Simon, B.; Tarascon, J.-M. *J. Electrochem. Soc.* **2008**, *155*, A158.
(26) Magasinski, A.; Zdyrko, B.; Kovalenko, I.; Hertzberg, B.; Burtovyy, R.; Huebner, C. F.; Fuller, T. F.; Luzinov, I.; Yushin, G. *ACS Appl. Mater. Interfaces* **2010**, *2*, 3004−10.
(27) Campion, C. L.; Li, W.; Lucht, B. L. *J. Electrochem. Soc.* **2005**, *152*, A2327.
(28) Chan, C. K.; Peng, H.; Liu, G.; McIlwrath, X. F.; Huggins, R. A.; Cui, Y. *Nat. Nanotechnol.* **2008**, *3*, 31−35.
(29) Chan, C. K.; Patel, R. N.; O'Connell, M. J.; Korgel, B. A.; Cui, Y. *ACS Nano* **2010**, *4*, 1443−1450.
(30) Wu, Y.; Cui, Y.; Huynh, L.; Barrelet, C. J.; Bell, D. C.; Lieber, C. M. *Nano Lett.* **2004**, *4*, 433−436.
(31) Park, M.-H.; Kim, M. G.; Joo, J.; Kim, K.; Kim, J.; Ahn, S.; Cui, Y.; Cho, J. *Nano Lett.* **2009**, *9*, 3844−7.
(32) Song, T.; Xia, J.; Lee, J.-H.; Lee, D. H.; Kwon, M.-S.; Choi, J.-M.; Wu, J.; Doo, S. K.; Chang, H.; Park, W. I/; Zang, D. S.; Kim, H.; Huang, Y.; Hwang, K.-C.; Rogers, J. A.; Paik, U. *Nano Lett.* **2010**, *10*, 1710−1716.
(33) Cui, L.-F.; Ruffo, R.; Chan, C. K.; Peng, H.; Cui, Y. *Nano Lett.* **2008**, *9*, 491−495.
(34) Ji, J.; Ji, H.; Zhang, L. L.; Zhao, X.; Bai, X.; Fan, X.; Zhang, F.; Ruoff, R. S. *Adv. Mater.* **2013**, *25*, 4673−4677.
(35) Kim, H.; Cho, J. *Nano Lett.* **2008**, *8*, 3688−91.
(36) Magasinski, A.; Dixon, P.; Hertzberg, B.; Kvit, A.; Ayala, J.; Yushin, G. *Nat. Mater.* **2010**, *9*, 353−8.
(37) McDowell, M. T.; Lee, S. W.; Ryu, I.; Wu, H.; Nix, W. D.; Choi, J. W.; Cui, Y. *Nano Lett.* **2011**, *11*, 4018−4025.
(38) Sim, S.; Oh, P.; Park, S.; Cho, J. *Adv. Mater.* **2013**, *25*, 4498−503.
(39) Wang, B.; Li, X.; Zhang, X.; Luo, B.; Zhang, Y.; Zhi, L. *Adv. Mater.* **2013**, *25*, 3560−5.
(40) Xu, Y.; Yin, G.; Ma, Y.; Zuo, P.; Cheng, X. *J. Mater. Chem.* **2010**, *20*, 3216.
(41) Guo, J.; Chen, X.; Wang, C. *J. Mater. Chem.* **2010**, *20*, 5035.
(42) Yun, M.; Jeong, K.; Lee, E.; Jin, B. *Korean J. Chem. Eng.* **2006**, *23*, 230−236.
(43) Chen, S.; He, G.; Hu, H.; Jin, S.; Zhou, Y.; He, Y.; He, S.; Zhao, F.; Hou, H. *Energy Environ. Sci.* **2013**, *6*, 2435−2439.
(44) Khriachtchev, L.; Kilpela, O.; Karirinne, S.; Keranen, J.; Lepisto, T. *Appl. Phys. Lett.* **2001**, *78*, 323−325.
(45) Khriachtchev, L.; Rasanen, M.; Novikov, S.; Pavesi, L. *Appl. Phys. Lett.* **2004**, *85*, 1511−1513.
(46) Nesheva, D.; Raptis, C.; Perakis, A.; Bineva, I.; Aneva, Z.; Levi, Z.; Alexandrova, S.; Hofmeister, H. *J. Appl. Phys.* **2002**, *92*, 4678−4683.
(47) Zhang, W.; Zhang, S.; Liu, Y.; Chen, T. *J. Cryst. Growth* **2009**, *311*, 1296−1301.
(48) Kingma, K.; Hemley, R. *Am. Mineral.* **1994**, *79*, 269−273.
(49) Karakassides, M.; Gournis, D.; Petridis, D. *Clay Miner.* **1999**, *34*, 429−438.
(50) Ferrari, A. C.; Meyer, J. C.; Scardaci, V.; Casiraghi, C.; Lazzeri, M.; Mauri, F.; Piscanec, S.; Jiang, D.; Novoselov, K. S.; Roth, S.; Geim, A. K. *Phys. Rev. Lett.* **2006**, *97*, 187401.
(51) Ferrari, A. C. *Solid State Commun.* **2007**, *143*, 47−57.
(52) Huang, Y.; Young, R. J. *Carbon* **1995**, *33*, 97−107.
(53) Dogan, F.; Joyce, C.; Vaughey, J. T. *J. Electrochem. Soc.* **2013**, *160*, A312−A319.
(54) Ge, M.; Rong, J.; Fang, X.; Zhang, A.; Lu, Y.; Zhou, C. *Nano Res.* **2013**, *6*, 174−181.
(55) Ma, D. D. D.; Lee, C. S.; Au, F. C. K.; Tong, S. Y.; Lee, S. T. *Science* **2003**, *299*, 1874−7.
(56) Egerton, R. F. *Rep. Prog. Phys.* **2009**, *72*, 016502.
(57) D'Aragona, F. *J. Electrochem. Soc.* **1972**, *119*, 948−951.
(58) Xia, Y.; Mrksich, M.; Kim, E.; Whitesides, G. *J. Am. Chem. Soc.* **1995**, *117*, 9576−9577.
(59) Knotter, D. M. *J. Am. Chem. Soc.* **2000**, *122*, 4345−4351.
(60) Li, W.; Li, H.; Zhang, Y.-M. *J. Mater. Sci.* **2009**, *44*, 2977−2984.
(61) Ge, M.; Rong, J.; Fang, X.; Zhou, C. *Nano Lett.* **2012**, *12*, 2318−2323.
(62) Li, J.; Dahn, J. R. *J. Electrochem. Soc.* **2007**, *154*, A156.
(63) Chen, X.; Li, X.; Ding, F.; Xu, W.; Xiao, J.; Cao, Y.; Meduri, P.; Liu, J.; Graff, G. L.; Zhang, J.-G. *Nano Lett.* **2012**, *12*, 4124−4130.
(64) Green, M.; Fielder, E.; Scrosati, B.; Wachtler, M.; Moreno, J. S. *Electrochem. Solid-State Lett.* **2003**, *6*, A75−A79.
(65) Allen, M. J.; Tung, V. C.; Kaner, R. B. *Chem. Rev.* **2010**, *110*, 132−145.
(66) Deheer, W.; Berger, C.; Wu, X.; First, P.; Conrad, E.; Li, X.; Li, T.; Sprinkle, M.; Hass, J.; Sadowski, M. *Solid State Commun.* **2007**, *143*, 92−100.
(67) Li, X.; Cai, W.; An, J.; Kim, S.; Nah, J.; Yang, D.; Piner, R.; Velamakanni, A.; Jung, I.; Tutuc, E.; Banerjee, S. K.; Colombo, L.; Ruoff, R. S. *Science* **2009**, *324*, 1312−4.
(68) Peng, Z.; Yan, Z.; Sun, Z.; Tour, J. M. *ACS Nano* **2011**, *5*, 8241−7.
(69) Bae, S.; Kim, H.; Lee, Y.; Xu, X.; Park, J.-S.; Zheng, Y.; Balakrishnan, J.; Lei, T.; Kim, H. R.; Song, Y. I.; Kim, Y.-J.; Kim, K. S.; Ozyilmaz, B.; Ahn, J.-H.; Hong, B. H.; Iijima, S. *Nat. Nanotechnol.* **2010**, *5*, 574−8.
(70) Kim, K. S.; Zhao, Y.; Jang, H.; Lee, S. Y.; Kim, J. M.; Kim, K. S.; Ahn, J.-H.; Kim, P.; Choi, J.-Y.; Hong, B. H. *Nature* **2009**, *457*, 706−10.